

# Interconnections between equilibrium topology and dynamical quantum phase transitions: a linearly ramped Haldane model

Utso Bhattacharya and Amit Dutta

Department of Physics, Indian Institute of Technology, 208016, Kanpur

In order to probe the role of equilibrium topology in dictating the behavior of Fisher Zeros (FZs) and dynamical quantum phase transitions (DQPTs) occurring in the subsequent temporal evolution of a quenched topological model, we invoke upon a linearly ramped Haldane model. Here, we investigate the temporal evolution of the final state of the Haldane Hamiltonian (evolving with time-independent final Hamiltonian) reached following a linear ramping of the staggered (Semenoff) mass term from an initial to a final value so chosen that the system is ramped from one non-topological phase to the other through a topological phase crossing two gapless Dirac points (DPs) in the process of quenching. Tracking the following time evolution of the final state, we observe that the areas of FZs do not cross the real time axis and hence no DQPTs exist in the limit of very fast quenches. On the contrary, in the extreme slow limit, we find a re-entrance of areas of FZs (across the real time axis) leading to non-analyticities in the time derivative of the dynamical “free energy” at four instants of real time for each set of FZs. We further establish the existence of a remarkable additional intermediate range of quenching rate for which the areas cross the real time axis only once even if the system is quenched across two DPs. Our study reveals that the appearance of the areas of FZs is an artefact of the non-zero (quasi-momentum dependent) Haldane mass ( $M_H$ ). Moreover, the characteristic rates marking the crossover between NO-DQPT to the intermediate and eventually to the re-entrant behavior are solely determined by the time-reversal invariant quasi-momentum points of the Brillouin zone where  $M_H$  vanishes. When  $M_H$  is altogether absent in the equilibrium Hamiltonian, the areas shrink to lines of FZs which cross the real time axis at specific instants of time where the “free energy” itself becomes non-analytic, thus resulting in an emergent effective one-dimensional behavior; additionally, there is no re-entrance, however slow may the quenching be. Furthermore, we argue that the topological nature of the equilibrium Haldane model fails to manifest itself in DQPTs in the infinite time Landau-Zener limit where excitation probability is insensitive to the presence of  $M_H$ . In essence, our study altogether establishes the existence of a profound connection between observed DQPTs and the equilibrium topology of the model considered.

## I. INTRODUCTION

The investigation of non-equilibrium many body quantum systems has always been a challenging task, both experimentally and theoretically. The recent experimental advances in realisation of closed condensed matter systems via cold atoms [1, 2] in optical lattices have paved the way for addressing unresolved fundamental problems in out of equilibrium strongly correlated systems. Henceforth, experimental studies have been performed to probe intriguing dynamical phenomena like the real time evolution of closed quantum systems in cold atomic gases, [3], prethermalization [4–6], light-cone like propagation of quantum correlations [7], light-induced non-equilibrium superconductivity and topological systems [8, 9] and many-body localization in disordered interacting systems [10]. In parallel, there have been a plethora of theoretical works on e.g., the growth of entanglement entropy following a quench [11], thermalization [12], light-induced topological matters [13, 14], dynamics of topologically ordered systems [15–17], periodically driven closed quantum systems [18–21] and many body localization [22, 23], to name a few. (For review, we refer to [24–28].)

One of the emerging features associated with a non-equilibrium quantum many body system is the possibil-

ity of dynamical quantum phase transitions in quenched closed quantum systems, introduced by Heyl *et al* [29]: here, non-analytic behavior occurs at critical times in the subsequent real time evolution (following the quench) generated by the time independent final Hamiltonian. To probe DQPTs in a closed quantum system, one prepares a desired final state  $|\psi_f\rangle$  of the system by quenching (changing slowly or rapidly) the parameters of the Hamiltonian usually from one phase to another across a quantum critical point (QCP) [30]. Then, this state is allowed to freely evolve in time with the time-independent final Hamiltonian ( $H_f$ ) up to a time  $t$  (measured from the instant when  $|\psi_f\rangle$  is prepared), before taking its overlap with the final state at the start of the free evolution. This so called Loschmidt overlap amplitude (LOA) is denoted by,  $G(t) = \langle\psi_f|e^{-iH_ft}|\psi_f\rangle$ , where the final state is not an eigenstate  $H_f$ . (It should be noted that throughout this paper the Planck constant  $\hbar$  is set equal to unity.) Generalization to the complex time ( $z$ ) plane yields  $G(z) = \langle\psi_f|e^{-H_f z}|\psi_f\rangle$  where  $z = \text{Re}[z] + it$ . Drawing a formal analogy between the inverse temperature ( $\beta$ ) and complex time ( $z$ ) [31–33], we notice that there exists a close similarity between the canonical partition function of an equilibrium classical system  $Z(\beta) = \text{tr}(\exp(-\beta H))$  and  $G(z)$  which can now be referred to as a dynamical partition function. By extending this analogy with equilibrium classical phase transitions further, one can now

define a quantity in the thermodynamic limit for a  $d$ -dimensional system with linear dimension  $L$ , called the dynamical free energy density

$$f(z) = - \lim_{L \rightarrow \infty} \frac{1}{L^d} \ln G(z).$$

One can then similarly look for zeros of  $G(z)$  (equivalently, non-analyticities in  $f(z)$ ) to find the so-called “Fisher zeros” (FZs) residing in the complex  $z$  plane. These zeros of the dynamical partition function ( $G(z)$ ) cover lines or areas (more specifically closely spaced points for a finite size systems which form continuous lines or dense areas in the thermodynamic limit) in the complex time ( $z$ ) plane (depending upon the *effective* dimensionality of the system under consideration). Consequently, when the lines (or areas) of FZs cross the imaginary (real time) axis at dynamical critical (real) times  $t_c = \text{Im}[z_c]$ , one observes DQPTs manifested in non-analyticities in  $\text{Re}[f(t)]$  (or its time derivative  $\text{Re}[f'(t)]$ ). Evidently, the LOA, i.e.,  $G(z)$  can only decay to zero, when the prepared many-body final state  $|\psi_f\rangle$  becomes orthogonal to its time evolved counterpart after free evolution with  $H_f$ .

The occurrence of DQPTs at specific instants of time following a rapid quench of a transverse Ising chain [34] across its QCP was established in Ref. [29] and the lines of FZs were indeed found to cross the real time axis at those instants. This observation has been independently confirmed through several works on quenched one-dimensional (1D) integrable and non-integrable systems [35–46]. Subsequent studies, however, have established that sudden quenching within the same phase of a system (both integrable and non-integrable) without ever encountering an equilibrium QCP may still give rise to DQPTs in some situations [47, 48]. Interestingly, in an attempt to characterise a DQPT through an order parameter, the crucial role played by topology has been exploited to define a dynamical topological order parameter (DTOP); the DTOP changes its integer value whenever the system dynamically crosses a critical time  $t_c$  signalling the occurrence of a DQPT [51].

DQPTs have also been observed for one dimensional systems when the state  $|\psi_f\rangle$  is prepared through slow quenching of a parameter of the initial Hamiltonian across QCP(s) [52]. Unlike the sudden quenching case, for slow quenching DQPTs survive in the subsequent evolution following quenches across two QCPs; moreover, the lines of FZs form a lobe like structure in the complex  $z$  plane which is also reflected in the temporal evolution of the DTOPs [53]. We note in passing that the study of a slow ramping across a QCP have gained importance because of the possibility of universal Kibble-Zurek scaling [54, 55] of the defect density and the residual energy in the final state reached after the quench [56, 57] (for review see, [24–26]).

Generalising to two dimensions, the possibility of the occurrence of DQPTs following a sudden quench from

the non-topological phase to the topological phase of the Haldane model and also from the gapped to the gapless phase of a Kitaev honeycomb model have been explored [49, 50]. These studies have shown that in stark contrast to that of the 1D case, the FZs (in this 2D case) cover areas instead of lines, producing non-analyticities in the time derivative of the dynamical free energy density (and *not* in the dynamical free energy density itself) at those instants of time where the boundaries of these areas cut the real time axis; as a result,  $\text{Re}[f''(t)]$  is discontinuous at those instants.

We further note that  $\text{Re}[f(t)]$  i.e.,  $(-1/L^d)\text{Re}[\ln \langle \psi_f | e^{-iH_f t} | \psi_f \rangle]$ , is closely related to the Loschmidt echo which has been studied extensively close to a QCP both in equilibrium [58–61] and non-equilibrium situations [62–65].  $\text{Re}[f(t)]$  can also be interpreted as the rate function of the return probability, so called because it can be connected to the singularities in the work distribution function corresponding to zero work following a double quenching process [29]; in such a process the initial Hamiltonian is quenched to the final Hamiltonian at  $t = 0$  and then quenched back to the initial one at a time  $t$ . The Loschmidt echo, interestingly, shares a close connection with several other fascinating aspects of non-equilibrium dynamics of quenched closed quantum system, e.g., work statistics [66, 67], entropy generation a emergent thermodynamics [68–70], still an experimental detection of a DQPT was lacking for quite some time. But very recently, Flaschner *et al.*, [71] has reported the first experimental observation of a DQPT using time-resolved state tomography to determine the dynamical evolution of a fermionic many-body state after a quench between two lattice Hamiltonians. In this work, the time evolution of a fermionic quantum gas in a hexagonal optical lattice was investigated after performing a sudden quench from a topologically trivial system into a Haldane-like system, which hosts both topologically trivial and nontrivial phases.

Consequently, this experiment motivates us, in this paper, to address the possibility of the occurrence of DQPTs following a slow (instead of a rapid) quench of a topological system. To this end, we invoke upon the paradigmatic Haldane model on a hexagonal lattice [72] (now an experimentally realized model [73], that for long has been providing the theoretical base for exploring topological insulators) to investigate the connection between the equilibrium topology and DQPTs following a slow (dictated by a rate) ramping of such a system. To the best of our knowledge, this is the first attempt to explore the DQPTs following slow quenches in a higher dimensional (equilibrium) topological system which may exhibit effective one-dimensionality in limiting situations. In this work, the (staggered) Semenoff mass term [74] in the topological Haldane model is slowly ramped via a linear quenching protocol with an inverse quenching rate  $\tau$  so that the system is quenched from one non-topological phase to the other across the topological phase in the process as shown in Fig. 1(a): To observe the DQPTs,

one then tracks the LOA of the final state evolving with the time-independent final Hamiltonian. Our study unearths the vital roles played by the parameter  $\tau$  and more fundamentally, by the Haldane mass in dictating the behavior of FZs and consequently in resultant DQPTs. We note that the slow ramping of the Haldane model has also been studied in the context of inducing topological transitions [75].

Let us summarize our main conclusions at the outset: we observe a re-entrant behavior of areas of FZs (if the rate  $\tau$  exceeds a critical value) across the imaginary  $z$ -axis (real time axis) which can be attributed to the slow passage of the system across two gapless Dirac points (DPs), i.e., QCPs, in the process of quenching. As a consequence, there exist four boundary points of the area of (one sector of) FZs those cut the imaginary (real time) axis resulting in four instants of real time where the first derivative of the dynamical free energy shows cusp singularities. It is remarkable that we also find the existence of an intermediate range of  $\tau$ , separating the NO-DQPT region (for very small  $\tau$ ) from the re-entrant region, for which the area of FZ cuts the real axis once; as a result, there are two boundary points and hence, only two instants of non-analyticities in free energy for a single set of FZs. The emergence of this intermediate region is only possible because of the fact that DPs lie inside the Brillouin zone, rather than at the corners. While the quenching rate  $\tau$  crucially determines the existence of three different behavior of FZs, the (quasi-momentum dependent) Haldane mass ( $M_H(\mathbf{k})$ ), which makes the Haldane model topologically non-trivial in the phases with non-zero Chern numbers, plays a more fundamental role: it is  $M_H(\mathbf{k})$  that renders the model anisotropic and hence the areas of FZs (2D behavior) appear. Furthermore, the critical values of  $\tau$  (which dictate the cross-over from the NO-DPT region to the intermediate and from the intermediate to the re-entrant region) are determined by the time reversal invariant momentum (TRIM) points of the Brillouin Zone (BZ) (as depicted in Fig. 1(b)) for which  $M_H(\mathbf{k}) = 0$ . In the situation, when the Haldane mass is altogether absent in the equilibrium model or does not affect the excitation probability during the quenching (e.g.,

the infinite time Landau Zener (LZ) limit), the FZs exhibit an emergent 1D behavior and form lines (*not* areas) which cut the real time axis at specific instants of time leading to non-analyticities in  $\text{Re}[f(t)]$  itself; furthermore there is no re-entrance of these lines in stark contrast with the observation reported for in 1D transverse XY chain [53].

Having introduced the motivation and summarised our key results, let us elaborate on the organization of the paper. In Sec. II, we introduce the Haldane model along with the quenching protocol emphasizing the role of the Haldane mass in rendering the model anisotropic. In Sec. III we present and analyze our main results illustrating the behavior of excitation probabilities and the areas of FZs for different values of  $\tau$ . In Sec. IV, we investigate some limiting situations: in Sec. IV A, we critically analyze the role of  $M_H(\mathbf{k})$  and illustrate how a dense area of FZs emerges from disjoint lines, while in Sec. IV B, we dwell on the infinite LZ limit where the role of  $M_H(\mathbf{k})$  is completely wiped out. Other than concluding comments presented in Sec. V, we also include two Appendices, for the sake of completeness. In Appendix A, a brief note on the Haldane model is provided and in Appendix B, we briefly mention the nature of DQPTs which occur following a slow quench across a single DP of the model.

## II. HALDANE MODEL AND QUENCHING SCHEME

Let us consider the 2D topological Haldane model on a hexagonal lattice comprised of two triangular sublattices  $A$  and  $B$  (refer to Appendix A for detail). The Haldane Hamiltonian is based on a graphene-like Hamiltonian but with a sublattice symmetry (SLS) breaking Semenoff mass (SM) term ( $M$ ) and a staggered magnetic field which manifests itself in the complex next nearest neighbour hopping. The presence of a periodic boundary condition enables us to write down the Hamiltonian in the quasi-momentum ( $k_x, k_y$ ) basis as,

$$\mathcal{H}(\mathbf{k}) = \begin{pmatrix} c_A^\dagger(\mathbf{k}) & c_B^\dagger(\mathbf{k}) \end{pmatrix} \begin{pmatrix} h_3(\mathbf{k}) & h_1(\mathbf{k}) + ih_2(\mathbf{k}) \\ h_1(\mathbf{k}) - ih_2(\mathbf{k}) & -h_3(\mathbf{k}) \end{pmatrix} \begin{pmatrix} c_A(\mathbf{k}) \\ c_B(\mathbf{k}) \end{pmatrix}, \quad (1)$$

where  $h_3(\mathbf{k}) = M + M_H(\mathbf{k})$  with  $M_H(\mathbf{k})$  being the quasi-momentum dependent Haldane mass given by

$$M_H(\mathbf{k}) = 2t_2 \sin(\phi) \left[ \sin(\mathbf{k} \cdot \mathbf{a}_2) - \sin(\mathbf{k} \cdot \mathbf{a}_1) + \sin(\mathbf{k} \cdot (\mathbf{a}_1 - \mathbf{a}_2)) \right], \quad (2)$$

that vanishes for  $t_2 = 0$  or  $\phi = 0$  and  $\mathbf{a}_1 = \frac{a}{2}(3, \sqrt{3})$  and  $\mathbf{a}_2 = \frac{a}{2}(3, -\sqrt{3})$ . We shall henceforth set the lattice

constant  $a = 1$  and use a rhomboidal BZ as shown in Fig. 1(b). The time reversal symmetry (TRS) in this model is broken by the phase factor  $\phi$  in the Haldane

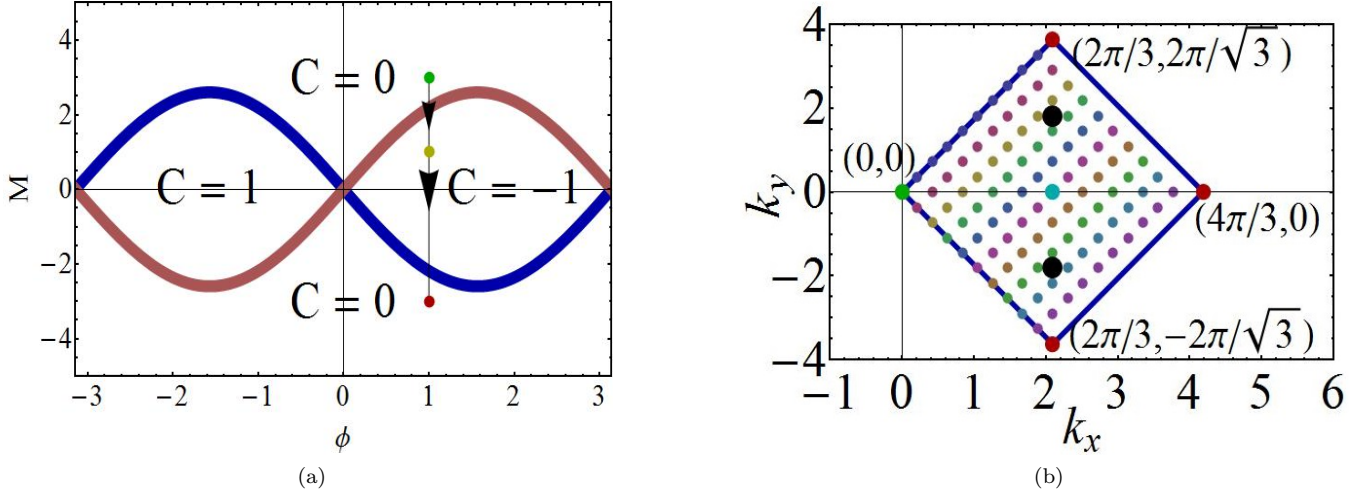


FIG. 1: (a) (Color online) The phase diagram of the Haldane model in  $M - \phi$  plane; topological phases and the non-topological phase correspond to Chern numbers  $C = \pm 1, 0$ , respectively. We employ a quenching scheme  $M(t) = -t/\tau$  with  $M_i = 3$  (green dot) and  $M_f = -3$  (red dot) with  $\phi = 1$ , so that the system is quenched across both the critical lines (i.e., gapless DPs) in the process of quenching. In Appendix B, we shall consider a slow ramping from  $M_i = 3$  (green dot) to  $M_f = 1$  (yellow dot). (b) The rhomboidal Brillouin zone (BZ) that we have chosen in this paper is illustrated for a  $10 \times 10$  system. The Dirac points are shown in black (biggest dots) while other small dots represent the points of the BZ. The four corner points and the highest symmetry point at the centre (with co-ordinates  $(2\pi/3, 0)$ ) marked by dots of medium size are time reversal invariant momentum (TRIM) points where  $M_H(\mathbf{k}) = 0$ ; while the left corner point  $(0, 0)$  (in green) and the central point (in cyan) are included in the BZ, other TRIM points (in red) are not.

mass term, originating from the staggered magnetic field and is positive for anticlockwise nearest neighbour hopping. The breaking of TRS indicates that the two Dirac points ( $\mathbf{K}$  and  $\mathbf{K}'$ ) in bare graphene spectrum are no longer time-reversed partners of each other as each of them sees a different Haldane mass  $M_H(\mathbf{k})$  depending on their quasi-momentum values, i.e.,  $\mathbf{K}$  or  $\mathbf{K}'$ . We will later see that the presence of this (Haldane) mass term (that depends on  $k_x$  and  $k_y$  explicitly) renders the model anisotropic and is essential for FZs to cover areas in the complex  $z$  plane. For a note on the model (1), we refer to the Appendix A.

We now perform a slow quench on the Haldane model, initially in the ground state  $|1_i\rangle$  of the initial Hamiltonian  $\mathcal{H}_i(\mathbf{k})$ , by linearly ramping the SLS breaking quasi-momentum independent SM term ( $M$ ) using the protocol  $M(t) = -t/\tau$  from an initial value  $M_i = 3$  to final value  $M_f = -3$  with  $\phi$  fixed to one as illustrated in Fig. 1(a). However, the results presented here would be in general true except for the special situations when  $\phi = 0$  and  $|M_i|, |M_f| \rightarrow \infty$ . In the former case, there is no non-trivial topology of the equilibrium model while the latter situation refers to the infinite time Landau-Zener problem [76, 77] where the role of topology is completely wiped out. In both the cases, we thus arrive at the problem of analyzing DQPTs in a linearly ramped gapped (Semenoff) graphene-like system as elaborated in Secs. IV A and IV B. Although, the finite time LZ problem can be studied within an analytical framework [78], the results

are not useful in the present context and consequently, we shall base our analyses and inferences on extensive numerical calculations of the finite time LZ problem.

In the process of ramping, the system passes through two gapless critical lines (see Fig. 1(a)) where the characteristic time scale (i.e., the relaxation time) diverges and hence, the condition for an adiabatic dynamics breaks down in their vicinity. One arrives at a final state (for the  $\mathbf{k}$ -th mode) at the end of the quenching:

$$|\psi_f(\mathbf{k})\rangle = u_f(\mathbf{k}) |1_f\rangle + v_f(\mathbf{k}) |2_f\rangle, \quad (3)$$

where  $|u_f(\mathbf{k})|^2 + |v_f(\mathbf{k})|^2 = 1$ ,  $|1_f\rangle$  and  $|2_f\rangle$  are the ground and excited states of the final Hamiltonian  $\mathcal{H}_f(\mathbf{k})$  with energy eigenvalues  $e_f^1(\mathbf{k})$  and  $e_f^2(\mathbf{k})$ , respectively; evidently,  $|v_{\mathbf{k}}|^2$  stands for the probability of excitation and is denoted by  $p_{\mathbf{k}}$  in the subsequent discussion.

Thus, the role of the slow quenching process is to prepare the system in the desired final state,  $|\psi_f(\mathbf{k})\rangle$  which then evolves in time with the final Hamiltonian ( $\mathcal{H}_f(\mathbf{k})$ ) yielding  $e^{-i\mathcal{H}_f(\mathbf{k})t'} |\psi_f(\mathbf{k})\rangle$ , where  $t' = t - t_f$  is measured from the instant when the final state is attained. One then immediately finds the LOA,  $G(t') = \prod_{\mathbf{k}} \langle \psi_f(\mathbf{k}) | e^{-i\mathcal{H}_f(\mathbf{k})t'} | \psi_f(\mathbf{k}) \rangle$ , which contains contribution from all the quasi-momenta ( $\mathbf{k}$ ) modes. Thus, to clarify, there are two kinds of evolution, one that takes  $|1_i\rangle$  at initial time  $t_i = 0$  to final quenching time  $t = t_f$  using the protocol  $M(t) = -t/\tau$ , to reach the state  $|\psi_f\rangle$ , which then evolves with time-independent  $\mathcal{H}_f(\mathbf{k})$ .



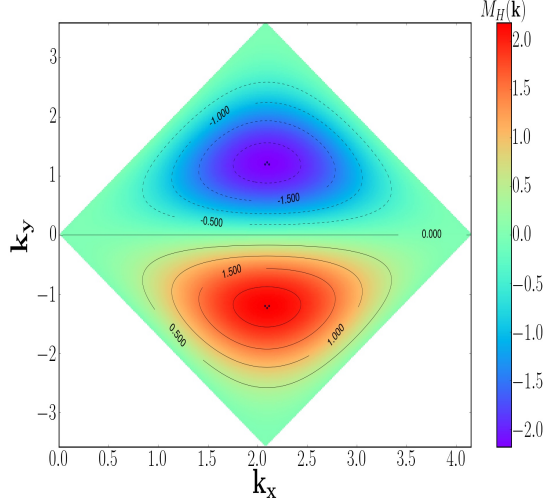


FIG. 2: The variation of the Haldane mass  $M_H(\mathbf{k})$  in the Brillouin zone (BZ) as a function of  $k_x$  and  $k_y$ . It is zero along the  $k_x$  axis when  $k_y = 0$  while it is positive (negative) in the lower (upper) half-plane. As a consequence of the time reversal invariance of this mode,  $M_H$  remarkably vanishes at all the TRIM points. Following any contour of fixed  $M_H(\mathbf{k})$  in the BZ, one can immediately conclude that the Haldane mass must explicitly depend on  $k_x$  and  $k_y$ .

Moving on to the complex  $z$ -plane, we now solve for the zeros of the dynamical partition function (FZs) ( $G(z) = 0$ ) to locate the dynamical critical points. It is then straightforward to show that the FZs are given by,

$$z_n(\mathbf{k}) = \frac{1}{e_f^2(\mathbf{k}) - e_f^1(\mathbf{k})} \left[ \log \left( \frac{p_{\mathbf{k}}}{1 - p_{\mathbf{k}}} \right) + i\pi(2n+1) \right] \quad (4)$$

where  $n = 0, \pm 1, \pm 2, \dots$  are integers; a particular value of  $n$  corresponds to one set of FZs and we shall essentially focus on the  $n = 0$  sector. The particle-hole symmetric nature of the Haldane Hamiltonian (1) demands that  $e_f^2(\mathbf{k}) = -e_f^1(\mathbf{k})$ , yielding

$$z_n(\mathbf{k}) = \frac{1}{2e_f^2(\mathbf{k})} \left[ \log \left( \frac{p_{\mathbf{k}}}{1 - p_{\mathbf{k}}} \right) + i\pi(2n+1) \right]. \quad (5)$$

These FZs when plotted in the complex  $z$ -plane for each value of  $k_x$  and  $k_y$  (for a fixed  $n$ ) may come together to form a line or cover a dense area depending upon the effective dimension of the system. Substituting  $p_{\mathbf{k}} = 1/2$  for the mode  $\mathbf{k} = \mathbf{k}^*$ , in Eq. (4) renders the real part of  $z_n$  zero while the imaginary part is given by  $i\pi(2n+1)/2e_f^2(\mathbf{k}^*) = it_c$ ; at these instants of real time,

$$t_c^{(n)} = \frac{\pi(n + \frac{1}{2})}{e_f^2(\mathbf{k}^*)} \quad (6)$$

one observes DQPTs, namely the non-analyticities (cusp singularities) in  $\text{Re}(f(t))$  or  $\text{Re}(f'(t))$ . Interestingly, the

critical times ( $t_c^{(n)}$ ) are inversely proportional to the energy (of the excited state)  $e_f^2(\mathbf{k}^*)$  of  $H_f$ . We also note that given the two-level nature of the problem the condition  $p_{\mathbf{k}^*} = 1/2$  implies an effective infinite temperature state of the final Hamiltonian for the mode  $\mathbf{k}^*$ . For brevity, we shall henceforth drop the subscript  $f$  in  $e_f^2(\mathbf{k})$ .

Let us now illustrate how the presence of a non-zero  $M_H(\mathbf{k})$  results in dense areas of FZs in the complex  $z$  plane. Given the two-dimensional nature of the Haldane Hamiltonian, one naturally expects that the values of  $k_x, k_y$  with the same excitation probability  $p_{\mathbf{k}}$  must lie within a continuum band or range. It is now important to analyze whether these particular values of  $\mathbf{k}$  for the entire range correspond to the same value of  $e^2(\mathbf{k})$ ; otherwise, Eq. (5) (for a given  $n$ ) ensures that the FZs corresponding to all these modes must lie at different points in the complex  $z$ -plane. Referring to the Hamiltonian (1), we find that  $e^2(\mathbf{k}) = \sqrt{(h_1^2(\mathbf{k}) + h_2^2(\mathbf{k}) + [M_f + M_H(\mathbf{k})]^2)}$ . We note that  $(h_1^2(\mathbf{k}) + h_2^2(\mathbf{k}))$  attains a constant value for a fixed  $\mathbf{k}$ ; consequently, it turns out to be absolutely necessary to explore the variation of  $M_H$  across the BZ to conclude about the functional dependence of  $e^2(\mathbf{k})$  on  $k_x$  and  $k_y$ . From Fig. 2, we immediately conclude that  $M_H(\mathbf{k})$  is anisotropic in  $k_x$  and  $k_y$  and has an explicit functional dependence on them. Therefore, this explicit dependence makes  $e^2(\mathbf{k})$  depend explicitly on  $k_x$  and  $k_y$  and hence FZs with different  $\mathbf{k}$  (corresponding to the same  $p_{\mathbf{k}}$ ) would lie at different points in the complex  $z$ -plane, resulting in an area of FZs for a particular  $n$ . Although the above argument holds true irrespective of the fact whether a  $\mathbf{k}^*$  exists or not, we shall now further elaborate the case when it does; the range of values of  $\mathbf{k}^*$  ( $k_x^*$  and  $k_y^*$ ) for which  $p_{\mathbf{k}^*} = 1/2$  would again result in different values of  $e^2(\mathbf{k}^*)$  which, as argued above, is an explicit function of  $k_x^*$  and  $k_y^*$ . Referring to Eq. (6), we conclude that FZs corresponding to different  $\mathbf{k}^*$  must touch the real time axis (imaginary  $z$ -axis) at different instants, which when extended to the whole complex  $z$  plane would lead to area of FZs. On the contrary, when  $M_H(\mathbf{k}) = 0$  in the equilibrium model, this explicit dependence on  $k_x$  and  $k_y$  disappears, and one gets an effective one-dimensional behavior where one observes lines of FZs, (*not* areas) and moreover, there is *no* re-entrance of FZs for any value of  $\tau$ . This issue will be further elaborated in Sec. IV A.

### III. RESULTS AND ANALYSES

In this section we present the main results of our paper and discuss three fascinating cases which illustrate how the appearance of FZs vary with the inverse rate of quenching  $\tau$  as we tune it from the sudden limit (when  $\tau \rightarrow 0$ ) to the extreme slow limit (when  $\tau \rightarrow \infty$ ) ramping the system linearly across two massless DPs (see Fig. 3).

As is evident from the figures in all situations  $p_{\mathbf{k}}$  is 1 at the DPs and smaller than 1 for modes away from them. Consequently, from Eq. (5), we conclude that FZs

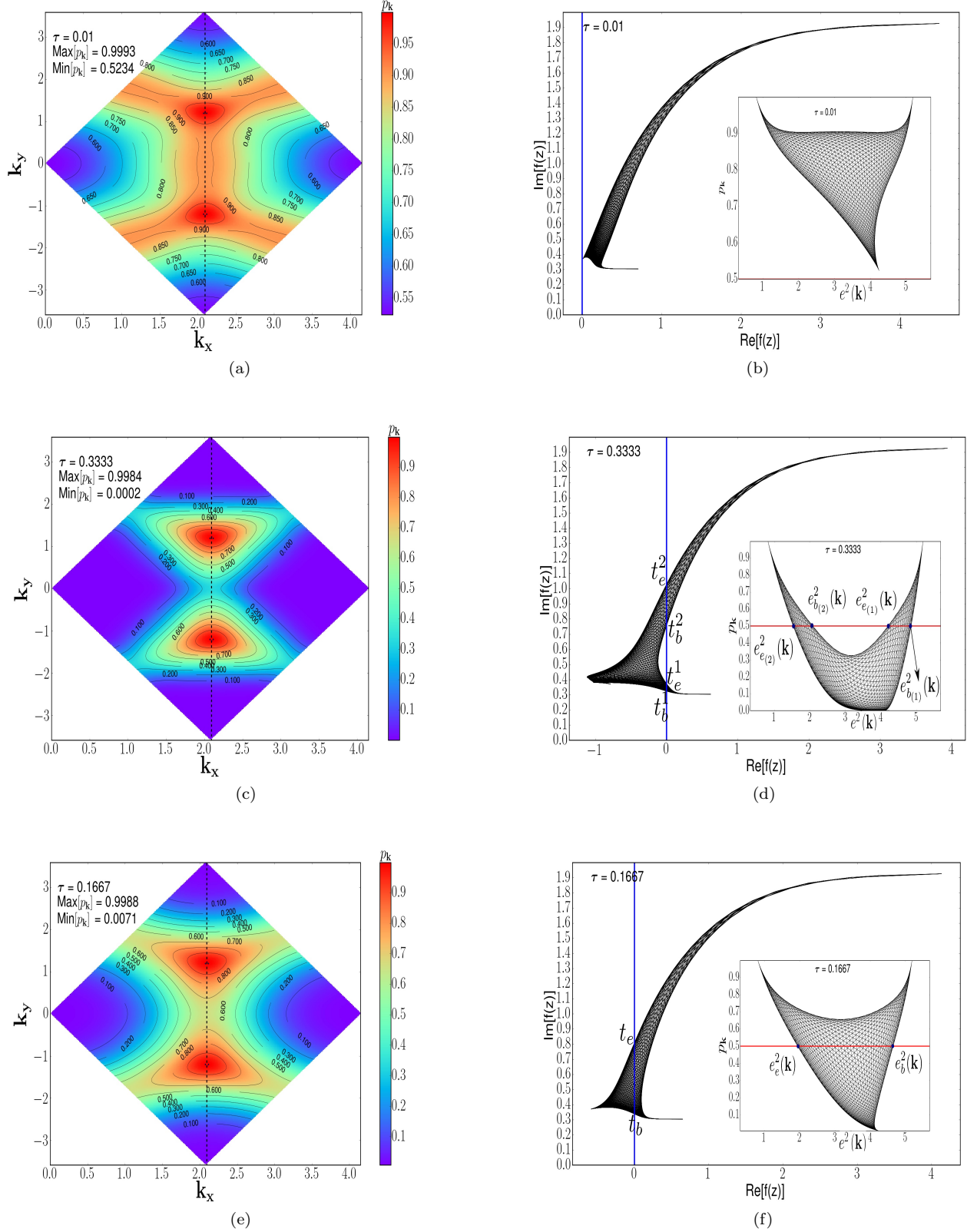


FIG. 3: (color online) This set of figures presents the variation of  $p_{\mathbf{k}}$  in the  $k_x - k_y$  plane and NO-DQPT, re-entrant and intermediate behaviours of FZs for the sector  $n = 0$  with  $M_i = 3, M_f = -3, \phi = 1$  and  $L = 100$ . In Figs. 3(a) and 3(b),  $\tau$  is small ( $< \tau_c^1$ ) so that the minimum value of  $p_{\mathbf{k}} \geq 1/2$  for all values of  $\mathbf{k}$  and the area never crosses the real axis. The inset of Fig. 3(b), validates the observation that there is no DQPT by showing that the area formed by  $e^2(\mathbf{k})$  does not touch the line  $p_{\mathbf{k}} = p_{\mathbf{k}^*} = 1/2$  for any value of the  $\mathbf{k}$ . On the contrary, Fig. 3(c) shows that in the extreme slow limit, i.e.,  $\tau > \tau_c^2$ ,  $p_{\mathbf{k}}$  becomes less than  $1/2$  along the dotted line connecting two DPs and there is a re-entrant behavior of FZs evident in Fig. 3(d): the inset shows four boundary points of  $e^2(\mathbf{k})$  on the line  $p_{\mathbf{k}} = 1/2$  leading to four instants of time  $t_b^1, t_e^1, t_b^2$  and  $t_e^2$ , (as obtained from Eq. (6)) where  $\text{Re}[f'(t')]$  is non-analytic (see Fig. 4(a)). For  $\tau_1^c < \tau < \tau_c^2$ , Fig. 3(e) shows that  $p_{\mathbf{k}}$  never becomes less than  $1/2$  along the dotted line and consequently, the area of FZs cross the real time axis only once (Fig. 3(f)): the inset shows the boundary points those lead to  $t_b$  and  $t_e$ , where  $\text{Re}[f'(t')]$  is non-analytic as shown in Fig. 4(b).

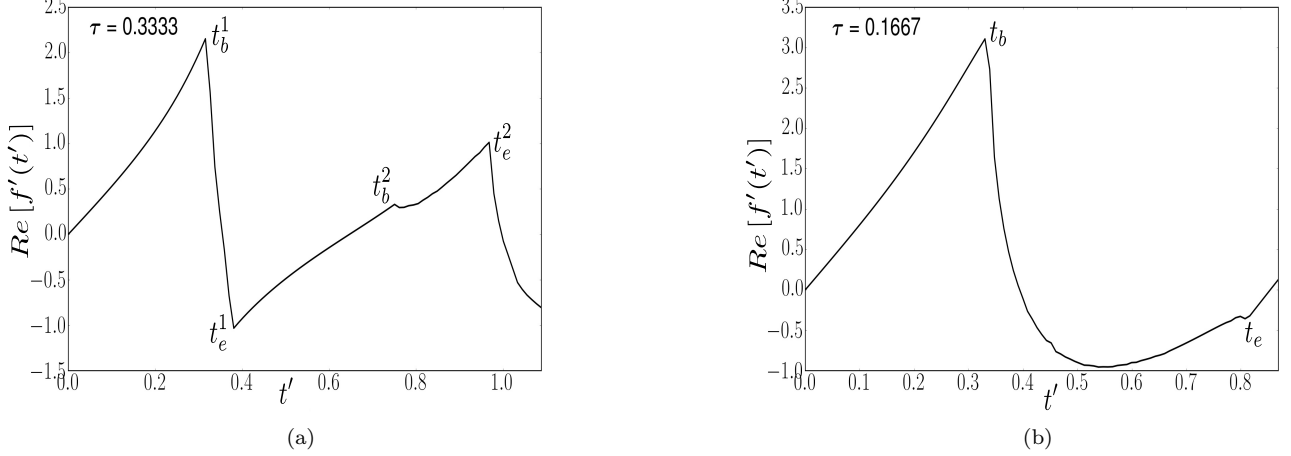


FIG. 4: The non-analyticities (cusp singularities) in  $\text{Re}[f'(t')]$  in the re-entrant and the intermediate situations (as predicted in Figs. 3(c)-3(f)) are shown in Figs. 4(a) and 4(b), respectively, for  $n = 0$ . Here, although we have used same  $\tau$ ,  $\phi$ ,  $M_i$  and  $M_f$  values as in Fig. 3,  $L$  is chosen to be 1000 to accentuate the instants of real time at which sharp non-analyticities appear.

corresponding to DPs would tend to  $+\infty$ , while for the modes with  $p_{\mathbf{k}} \rightarrow 0$  the FZs would approach  $-\infty$ , yielding the possibility of FZs extending from  $-\infty$  to  $+\infty$  in the thermodynamic limit.

Let us first consider the extreme limit, i.e., the sudden quenching limit where the value of  $\tau \rightarrow 0$ . Therefore, although the system is quenched across both the QCPs, as shown in Fig. 3(a), the rapid rate of quenching never allows the minimum value of  $p_{\mathbf{k}^*}$  to become less than  $1/2$ ; consequently, area of FZs never cross the real time axis (as shown in Fig. 3(b)) and hence there is no non-analyticity either in  $\text{Re}[f(t)]$  or in its time derivative resulting in a complete absence of DQPTs.

Now considering the other extreme limit, i.e., the slow limit (see Fig. 3(c)), let us follow the contour plot of the excitation probability,  $p_{\mathbf{k}}$  along the  $k_x = \frac{2\pi}{3}$  line. Every time the system goes from a value of  $p_{\mathbf{k}} = 0$  to  $p_{\mathbf{k}} = 1$ , the excitation probability attains the value of  $p_{\mathbf{k}} = p_{\mathbf{k}^*} = 1/2$ . These values of  $k_x^*$  and  $k_y^*$  form two lobes (closed contours) of  $p_{\mathbf{k}^*} = 1/2$  centred around the two DPs. Referring to Eq. (4) and the discussion following it, one can explain the observation, as shown in Fig. 3(d), that the area of FZs (for  $n = 0$ ) crosses the real time axis twice which means that their boundaries cross four times; this remarkable behavior of the areas of FZs is referred to as re-entrances. Referring to the inset of Fig. 3(d), the line  $p_{\mathbf{k}^*} = \frac{1}{2}$  cuts the area generated by  $e^2(\mathbf{k})$  multiple times leading to a continuum band or range of  $\mathbf{k}^*$  with four boundary values of  $e^2(\mathbf{k}^*)$ ; these boundary values when substituted in Eq. (6) (with  $n = 0$ ) lead to four time scales  $t_b^1$ ,  $t_e^1$ ,  $t_b^2$  and  $t_e^2$ , corresponding to upper and lower lobes of  $p_{\mathbf{k}^*} = 1/2$  contours. Consequently,  $\text{Re}[f'(t)]$  shows cusp singularities at these instants of time (see Fig. 4(a)). Again, from Eq. (6), we immediately conclude that  $t_b^1$  and  $t_b^2$  corresponds to the maximum of the highest and the lowest energy bands, while  $t_e^1$  and  $t_e^2$  are given in

terms of the minimum of these two energy bands.

Focussing on the  $n = 0$  sector, we have so far analysed two limits of  $\tau$ : extreme fast ( $\tau < \tau_1^c$ ), when there is no DPT and the extreme slow ( $\tau > \tau_2^c$ ) when there are re-entrances. But the most intriguing situation arises at intermediate values of  $\tau = \tau_i$ , where  $\tau_1^c < \tau_i < \tau_2^c$ . Here, although the system passes through two critical points, the FZs (for  $n = 0$ ) collate to form an area in the complex  $z$  plane whose boundaries rather interestingly cross the real time axis at two pairs of time instants only (see Fig. 3(f)), in stark contrast with re-entrance of FZs shown in Fig. 3(d). Carefully analysing this scenario from Fig. 3(e), we note that the crucial difference with the re-entrance case happens to be the fact that there exists only a *single*  $p_{\mathbf{k}} = p_{\mathbf{k}^*} = 1/2$ , curve encircling both the DPs (QCPs). Focusing on the variation of  $p_{\mathbf{k}} = 1/2$  with  $k_y$  on the line  $k_x = 2\pi/3$ , we conclude that  $p_{\mathbf{k}}$  gradually becomes smaller than  $1/2$  with distance from DPs on either side (of the DPs) but is definitely greater than  $1/2$  between them. The upper critical value  $\tau_2^c$  is that value of  $\tau_i$  for which the  $p_{\mathbf{k}}$  becomes  $1/2$  between the two DPs on the  $k_x = 2\pi/3$  line at the point  $k_y = 0$ : for  $\tau > \tau_2^c$ , we see the formation of two  $p_{\mathbf{k}} = p_{\mathbf{k}^*} = 1/2$  contours encircling the two DPs emerging from the single contour for  $\tau < \tau_2^c$ . Therefore, in the intermediate regime, the value of  $\tau_i$  is such that there is only one  $p_{\mathbf{k}} = p_{\mathbf{k}^*} = 1/2$  lobe enclosing the two DPs resulting in the creation of a single area of FZs. Once again, recalling Eq. (6), the lower (upper) boundary of the area that crosses the real time axis is determined by the maximum (minimum) of  $e^2(\mathbf{k})$  on the line  $p_{\mathbf{k}} = 1/2$  (inset of Fig. 3(f)) and one observes cusp singularities in  $\text{Re}[f'(t)]$  only at two instants of real time as shown in Fig. 4(b).

The question that naturally arises at this point is what determines the crossover values of the rate  $\tau$  for which the transitions between the three different regions occur and

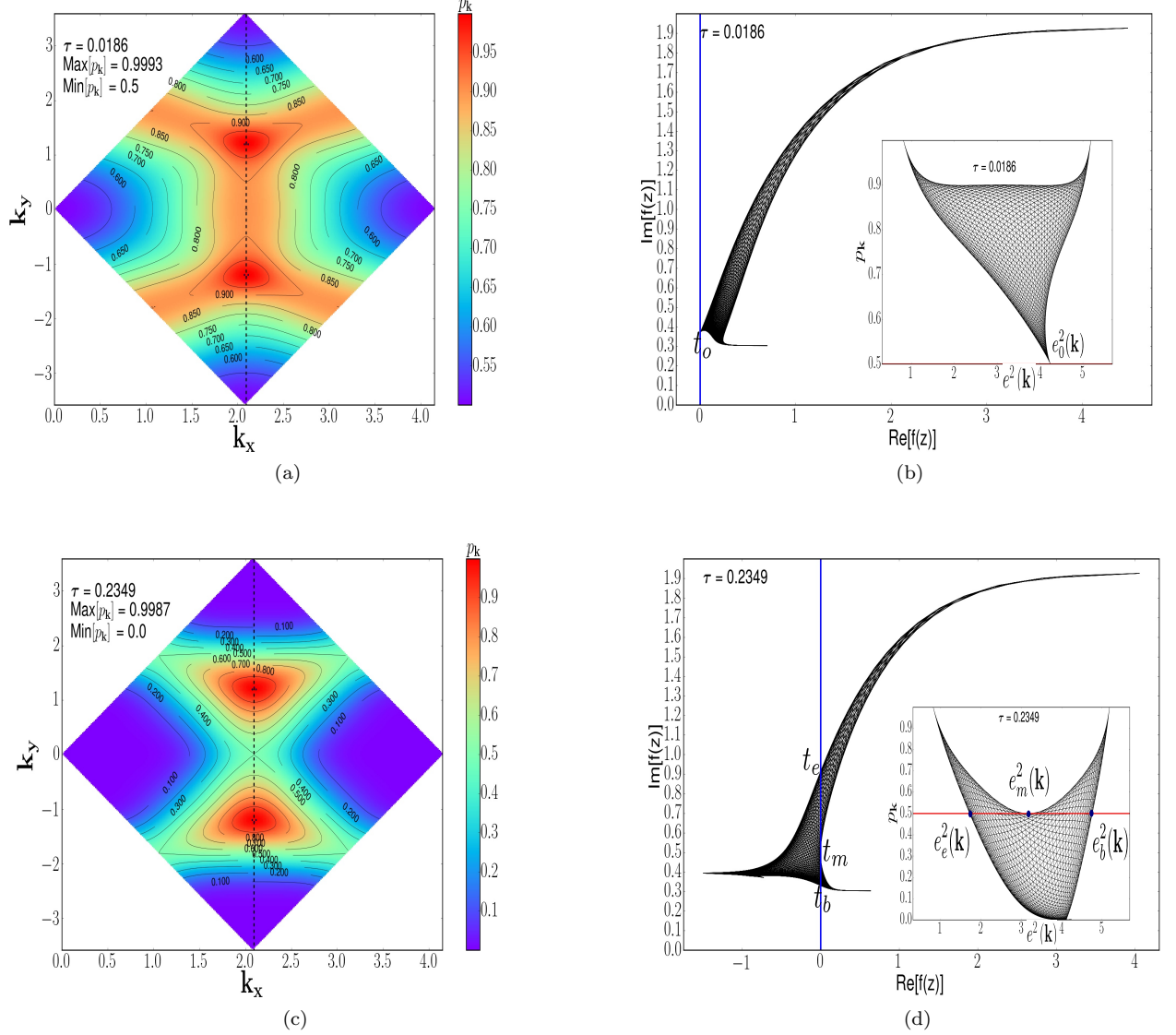


FIG. 5: (color online) This set of figures presents the scenario occurring at the critical values of  $\tau$ , namely,  $\tau_c^1$  and  $\tau_c^2$ , with  $M_i = 3, M_f = -3, \phi = 1$  and  $L = 100$ . As shown in Fig. 5(a), at  $\tau = \tau_c^1$ , the excitation probability  $p_{\mathbf{k}}$  becomes  $1/2$  for the mode  $k_x = k_y = 0$  (the TRIM point at the corner of BZ in Fig. 1(b)) for which  $M_H = 0$ . Fig. 5(b) shows that the area of FZs touch the imaginary (real time) axis for this mode at the instant  $t_m$ ; the inset shows that  $e^2(\mathbf{k})$  touches the  $p_{\mathbf{k}} = 1/2$  line for this momentum mode. On the contrary, at  $\tau = \tau_c^2$  (Fig. 5(c)),  $p_{\mathbf{k}}$  just becomes  $1/2$  for the TRIM point at the centre of the BZ. Consequently, as shown in (Fig. 5(d)), the internal boundary of the area of FZs touches the real time axis for this mode; this is more transparently depicted in the inset, there is an additional boundary point for the energy  $e_m^2(\mathbf{k})$  (that corresponds to the instant  $t_m$ ) when compared to the inset of the Fig. 3(f).

how do these scales depend on the parameter  $\phi$  (or specifically  $M_H$ ). Recalling the fact that the  $p_{\mathbf{k}}$  is the smallest for the modes  $\mathbf{k}$  farthest from the gapless DPs, we focus on the TRIM point at  $k_x = k_y = 0$  (with  $M_H(\mathbf{k}) = 0$ ), that has minimum value  $p_{\mathbf{k}}$  and is fully included in the BZ shown in Fig. 1(b). Since the minimum value of  $p_{\mathbf{k}}$  must at least be  $1/2$  for DPTs to appear, the condition  $\text{Min}[p_{\mathbf{k}}] = 1/2$ , at this farthest mode determines the scale  $\tau_c^1$  as shown in Fig. 5(a).  $\text{Min}[p_{\mathbf{k}}]$  at this TRIM, is inde-

pendent of  $M_H$ , and evidently so is  $\tau_c^1$ . On the other hand, the transition from the intermediate to the re-entrant phase taking place at  $\tau_c^2$  occurs when the  $p_{\mathbf{k}} = 1/2$  lobe enclosing the two DPs separate out at the other TRIM point  $k_x = 2\pi/3, k_y = 0$  (closest to the two DPs and located at the centre of BZ) with zero Haldane mass, to form two distinct lobes enclosing one DP each (Fig. 5(c)). When the value of  $\tau$  is insufficient to make the  $p_{\mathbf{k}}$  at this mode less than  $1/2$ , the system remains in

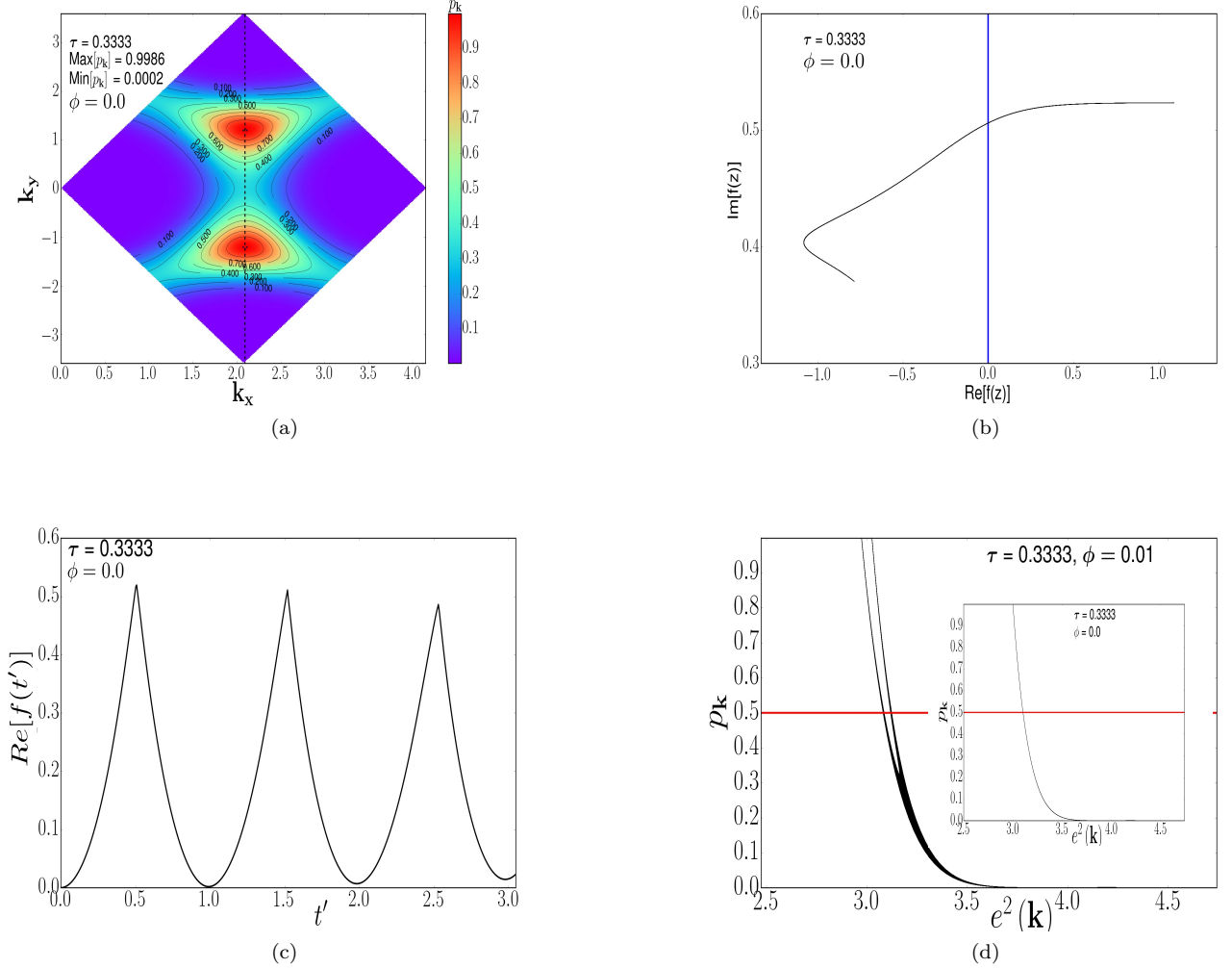


FIG. 6: (color online) These figures demonstrate the effective 1D behavior that emerges when the parameter  $\phi$  and consequently,  $M_H$  vanishes; we choose  $\tau = .3333$ , so that for  $\phi \neq 0$ , there is a re-entrant behavior as presented Figs. 3(c) and 3(d). Fig. 6(a) shows that the excitation probability  $p_{\mathbf{k}} \sim 1$ , around both the DPs. Nevertheless, as shown in Fig. 6(b), the FZs constitute a line rather than an area; furthermore, the re-entrant behavior completely disappears. As elaborated in the text, in Fig. 6(c)), we show that there exists sharp non-analyticities in  $\text{Re}[f(t')]$  itself at different instants of time and we choose  $n = 0, 1$  and  $2$ . In Fig. 6(d), it is illustrated that even for very small  $\phi$ , there are four boundary points of  $e^2(\mathbf{k})$  on the line  $p_{\mathbf{k}^*} = 1/2$ , which shrink to one point as soon as  $\phi$  vanishes (inset).

the intermediate phase, but at  $\tau = \tau_c^2$ ,  $p_{\mathbf{k}}$  becomes  $1/2$  at this mode and the system enters the re-entrant phase for  $\tau > \tau_c^2$ . Hence, this mode being independent of  $M_H$  again keeps  $\tau_c^2$  invariant under the variation of  $\phi$ . We further emphasize that both  $\tau_c^1$  and  $\tau_c^2$  are determined by TRIM points, and hence, are independent of the system size as long as it is ensured that the numerical scheme sharply includes these points while enumerating different modes of the BZ. Of course, these critical values do not get altered in the thermodynamic limit.

Having established the independence of  $\tau_c^1$  and  $\tau_c^2$  on the parameter  $\phi$ , we shall now proceed to argue how the area of FZs (for the sector  $n = 0$ ) should look at these critical rates  $\tau = \tau_c^1$  and  $\tau_c^2$ . Note that at  $\tau = \tau_c^1$ ,  $p_{\mathbf{k}}$

corresponding to the mode  $k_x = 0, k_y = 0$  becomes  $1/2$  and it is *only* the FZ corresponding to this particular point of the area which touches the real time axis as shown in Fig. 5(b). On the contrary, at  $\tau = \tau_c^2$ , the internal boundary of the area of FZs touches the real axis for the mode  $k_x = 2\pi/3, k_y = 0$ , in addition to already existing two crossings due to the intermediate behaviour. In short, the area crosses the real time axis for two momenta and additionally touches it for the above TRIM point (Fig. 5(d)). When  $\tau$  exceed  $\tau_c^1$  ( $\tau_c^2$ ) even infinitesimally, the intermediate (re-entrant) behaviour as shown in Figs. 3(c)-3(f) sets in.



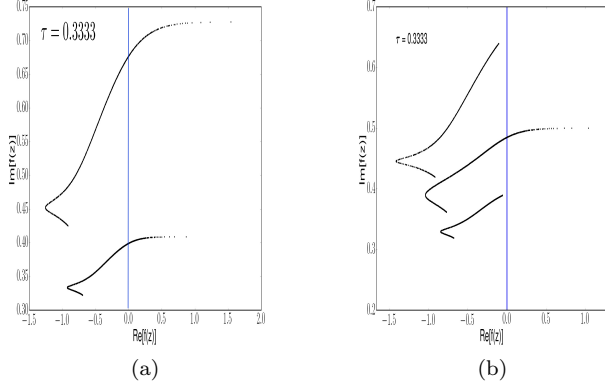


FIG. 7: (a) The FZs when  $M_H(\mathbf{k})$  assumes two constant values (with different signs) at two DPs; we obtain two disjoint lines of FZs both crossing the real time axis at two different instants. (b) This refers to a hypothetical situation where the Haldane mass assumes three constant values in three regions of the BZ as elaborated in the text and consequently one obtains three disjoint lines.

#### IV. LIMITING SITUATIONS: EFFECTIVE ONE DIMENSIONALITY

##### A. Formation of areas of FZs due to $M_H(\mathbf{k})$ :

We have already demonstrated that the non-zero Haldane mass, which renders the problem anisotropic, plays a crucial role in generating areas of FZs in the complex  $z$  plane. Furthermore, it vanishes for the TRIM points which determine the characteristic values of  $\tau$ , i.e.,  $\tau_1^c$  and  $\tau_2^c$ . In this section, we shall revisit the crucial role played by  $M_H(\mathbf{k})$  by considering some limiting and hypothetical situations. Let us first analyze the situation when the Haldane mass altogether vanishes, (i.e., the parameter  $\phi = 0$ ) so that the equilibrium model is simply a massive Dirac Hamiltonian which does not possess any non-trivial topology (see Fig. 6). Although the results presented Fig. 6 are obtained for the lattice model, to obtain an intuitive understanding of the results, we resort to the continuum limit: one can then recast the Hamiltonian (1) in the vicinity of DPs with  $M_H(\mathbf{k}) = 0$ , in the form:

$$\mathcal{H} = \begin{pmatrix} M(t) & k_x + ik_y \\ k_x - ik_y & -M(t) \end{pmatrix}, \quad (7)$$

where  $k_x, k_y$  are measured from each DP. The SM,  $M(t) = -t/\tau$  is ramped from  $M_i = +3$  to  $M_f = -3$  as shown in 1(a) but with  $\phi = 0$ ; the system is thus quenched through two gapless DPs (which in the present case are time reversed partners of each other). Although referring to Fig. 6(a), we find  $p_{\mathbf{k}} = 1$  at both DPs, FZs (for the sector with  $n = 0$ ) form a single line in the  $z$ -plane (Fig. 6(b)) cutting the real time axis only once; the

re-entrant behavior observed in Fig. 3(d) also completely disappears because the lines of FZs associated with the upper and lower DPs fall on top of each other coalescing into the observed single line.

To comprehend this observation, let us note in the present case, one can argue that the modes  $\mathbf{k}^*$  (for which  $p_{\mathbf{k}^*} = 1/2$ ), satisfy the condition  $|\mathbf{k}^*|^2 = (k_x^*)^2 + (k_y^*)^2 = \text{constant}$ . More importantly,  $e^2(\mathbf{k}) = \sqrt{|\mathbf{k}|^2 + M_f^2}$  is no longer anisotropic, rather depends only on  $|\mathbf{k}|$ . Evidently, the entire range of  $\mathbf{k}^*$  leads to the same value of  $e^2(\mathbf{k}^*)$ . Consequently, the system is effectively one-dimensional of real time (for each  $n$ ) at which  $\text{Re}[f(t)]$  itself shows a cusp singularity, as presented in Fig. 6(c), with a discontinuous change in its first derivative. Even for an infinitesimally small  $\phi$ , the areas of FZs reappear along with the re-entrant behavior (Fig. 6(d)).

Let us now extend to the situation when the Haldane mass is  $M_H^\alpha(\mathbf{k})$  in the continuum limit is positive at one DP and negative at the other. Expanding around these DPs labelled by the index  $\alpha = \pm 1$ , we arrive at two Hamiltonians:

$$\mathcal{H}^\alpha = \begin{pmatrix} M(t) + M_H^\alpha & k_x + ik_y \\ k_x - ik_y & -(M(t) + M_H^\alpha) \end{pmatrix}, \quad (8)$$

where the Haldane mass  $M_H = -3t_2\alpha \sin \phi$ . In this case, though  $M_H$  is independent of the magnitude of the quasi-momentum, the two DPs sense different  $M_H$ . This is reflected in the behavior of FZs, which now form two disjoint lines corresponding to the sector  $n = 0$  as shown in Fig. 7(a), which cut the real axis at two different instants of time. We emphasise that an area of FZs does not appear in this case!

The example above can also be viewed as a special situation where  $M_H$  is positive in the upper half of the BZ while negative in the lower half. This can be further extended to an artificial situation where  $M_H$  assumes three different values along three regions parallel to the  $k_x$ -axis of the BZ where the central region extends from  $k_y = \pi/\sqrt{3}$  to  $k_y = -\pi/\sqrt{3}$  with a constant Haldane mass  $M_H^2$ , whereas the regions above and below it have constant masses  $M_H^1$  and  $M_H^3$ , respectively, with the condition  $M_H^1 > M_H^2 > M_H^3$ . In this case, one finds three disjoint lines of FZs as shown in Fig. 7(b). When generalized to  $n$  similar stripes with constant mass  $M_H^{(n)}$  for the  $n$ -th stripe, more and more disjoint lines of FZs appear. Equipped with this interesting observation, one can now view the continuous variation of the  $M_H(\mathbf{k})$  across the BZ (Fig. 2), as a limiting situation when area of these regions becomes infinitesimal; in a such scenario these disjoint lines coalesce to form a quasi-area which becomes a real dense area in the thermodynamic limit. This provides an intuitive explanation of how the anisotropy in  $M_H(\mathbf{k})$  generates areas of FZ from otherwise disjoint lines.

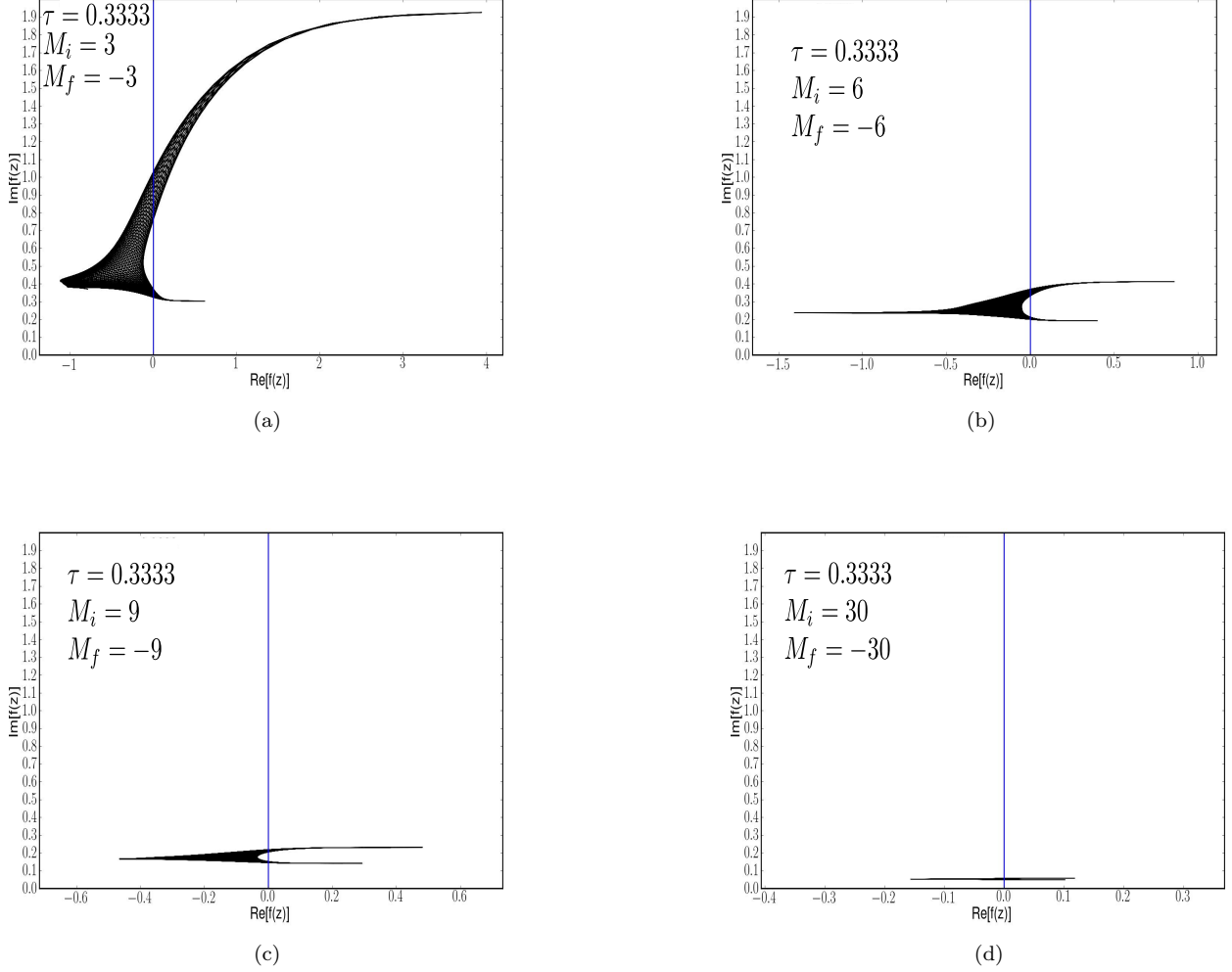


FIG. 8: (color online) Here, we illustrate how the role of Haldane mass is wiped out as we approach the infinite time Landau-Zener limit by gradually increasing  $M_i$  and  $|M_f|$ . Analyzing Figs. 8(a)-8(d), one can conclude that when  $M_i$  and  $|M_f|$  both are increased to very high magnitudes, the FZs constitute a line and an effective 1D behavior similar to that in Fig. 6(b) emerges, and therefore there are cusp singularities in the  $\text{Re}[f(t')]$  itself.

### B. The infinite time Landau-Zener limit

Let us now consider a quenching protocol in which the staggered mass is quenched from negative infinity to positive infinity (or the other way round) in a linear fashion, i.e., the infinite time LZ limit. In this limit, the LZ transition formula where  $p_{\mathbf{k}}$ 's are determined solely by the off-diagonal terms of the Hamiltonian and the inverse quenching rate  $\tau$  [76, 77], holds true. Referring to Eq. (1) and using the LZ transition formula, the excitation probability for the mode  $\mathbf{k}$  is found to be of the form  $p_{\mathbf{k}} = \exp[-\pi\tau(h_1^2(\mathbf{k}) + h_2^2(\mathbf{k}))]$  (which reduces to  $\exp[-\pi\tau(k_x^2 + k_y^2)]$  in the continuum limit [79]). Since the Haldane mass plays no role in determining  $p_{\mathbf{k}}$ 's, the situation is again effectively one dimensional with the lines of FZs (corresponding to any  $n$ ) crossing the real axis at only one instant of real time and there is no re-

entrant behavior for any value of  $\tau$ . This is illustrated in Figs. 8(a)-8(d) that when  $M_i$  and  $|M_f|$  are gradually increased to higher and higher magnitudes, two branches of the lobe of FZs corresponding to  $n = 0$  eventually fall on top of each other forming a line. We therefore conclude that it is the finite time nature of the quenching protocol which captures the topological nature of the Haldane model and gets reflected in the behavior of DQPTs.

## V. CONCLUSION

Exploiting the two band nature of the topological Haldane model which enables us to employ extensive investigations of finite time LZ problems, we establish a profound connection between the equilibrium topology of the Haldane model and subsequent DQPTs following a



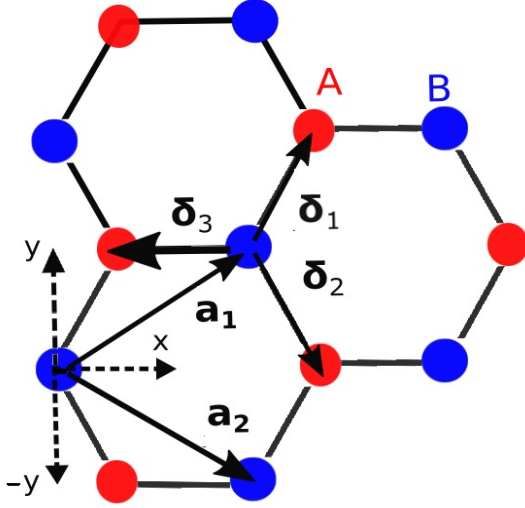


FIG. 9: A hexagonal lattice on which the topological Haldane model resides with  $\mathbf{a}_1$  and  $\mathbf{a}_2$  as the lattice vectors.

linear ramping of the SM from one non-topological phase to the other. Other than the re-entrance of areas of FZs (across the real time axis) in the extreme slow limit which is an artefact of quenching across two DPs, we establish the existence of an intermediate range of the quenching rate for which areas of FZs cross the real axis only once leading to two (instead of four as in the re-entrant case) instants of non-analyticities in  $\text{Re}[f(t')]$  for a fixed value of  $n$ . This intermediate region, which does not show up in the case of the transverse Ising chain [53], exists only because of the position of the DPs inside the BZ; this allows  $p_{\mathbf{k}}$  to vanish above (below) the upper (lower) DP along the line  $k_y = 2\pi/3$  while keeping it always greater than  $1/2$  between them for appropriate values of  $\tau$ .

The quasi-momentum dependent Haldane mass, which breaks the time-reversal invariance, thus rendering the equilibrium Haldane model topological, plays the most crucial role: it is the presence of a non-zero  $M_H(\mathbf{k})$  that results in the appearance of areas of FZs in the complex  $z$  plane as well as the re-entrant behavior in the extreme slow limit. When  $M_H(\mathbf{k})$  is switched off or is inconsequential in determining the excitation probability  $p_{\mathbf{k}}$  (as in the infinite time LZ situation), the areas shrink to lines of FZs giving rise to an emergent one dimensional behavior with non-analyticities in  $\text{Re}[f(t')]$  itself (and discontinuities in  $\text{Re}[f'(t')]$ ) at those instants when these lines cut the real axis; furthermore, the re-entrant behavior completely disappears even in the extreme slow limit. Focussing on the re-entrant situation, if the value of  $M_H(\mathbf{k})$  (and consequently the anisotropy of the momenta modes of the model) is slowly reduced, the areas corresponding to two branches of a lobe (for a given  $n$ ) become thinner and thinner approaching two lines which eventually fall on top of each other when  $M_H(\mathbf{k}) = 0$ ; this has also been transparently demonstrated by grad-

ually approaching the infinite LZ limit (in which  $p_{\mathbf{k}}$  is completely independent of  $M_H(\mathbf{k})$ ) starting from the finite LZ case. We have also illustrated by considering hypothetical situations when the BZ is divided into regions with different (but constant within a region)  $M_H$ , how otherwise disjoint lines of Fisher zeros coalesce into dense areas in the real model with continuously varying  $M_H$  in the thermodynamic limit. Crucially, the critical rates  $\tau_1^c$  and  $\tau_2^c$ , marking the crossover between the NO-DPT, intermediate and re-entrant behavior of FZs are solely determined by the TRIM point included in the BZ for which  $M_H = 0$ , thereby, further emphasising the immense importance of the Haldane mass in dictating the nature of DQPTs. It is also noteworthy that the Haldane mass (which generates the equilibrium topology) also plays an equally important role in dictating the nature of these out of equilibrium DQPTs, as elucidated above, for all quenching protocols including the extreme, i.e., sudden quenching limit.

We would like to emphasize that given the recent experimental observation of DQPTs [71], it would be possible to verify the predictions presented here experimentally. It should also be noted that the finite time LZ limit, on which we focus on, is more feasible to experimental verification than an infinite LZ limit. Furthermore, there has also been a recent work in which Yang-Lee zeros have been observed experimentally [80]. Our work, naturally, opens up the possibility of further research in several new directions. One such example would be to explore the role of equilibrium topology in determining DQPTs in higher dimensional quenched topological models. Another intriguing question that inevitably needs to be addressed would be the effect of the edge states appearing in equilibrium topological models with open boundary condition, on the DQPTs described here.

### Acknowledgements

We acknowledge interesting discussions with Shraddha Sharma. We also thankfully acknowledge G. Baskaran and A. Polkovnikov for critical comments. We also acknowledge discussions AD acknowledges financial support from DST, India.

### Appendix A: A brief note on the Haldane model

We consider a 2D model on a hexagonal lattice comprised of two triangular sublattices  $A$  and  $B$  as shown in Figure 9. It can be understood as the composition of a nearest neighbour tight binding graphene-like Hamiltonian along with a Haldane mass ( $M_H$ ) and sublattice symmetry (SLS) breaking Semenoff mass ( $M$ ) term, with

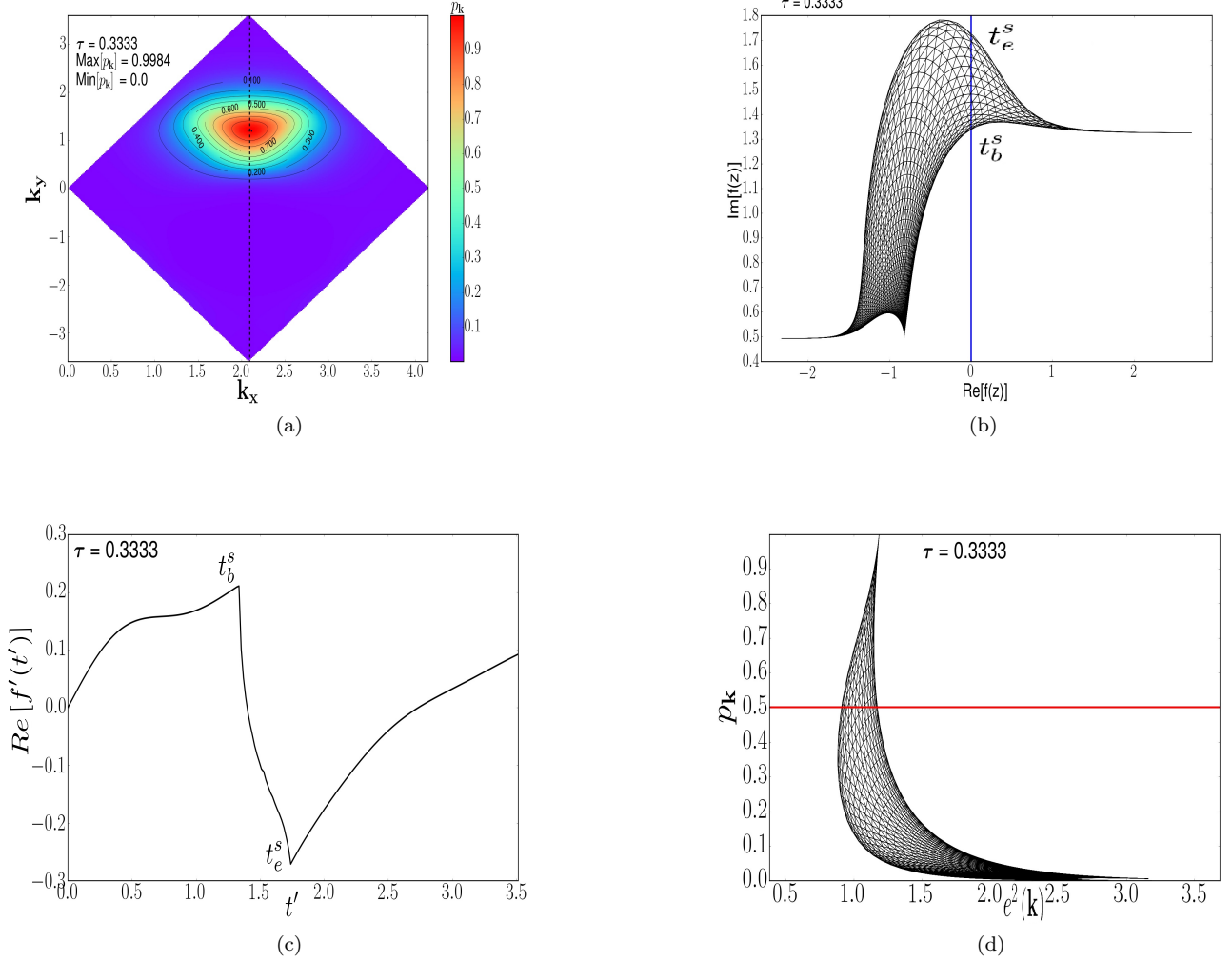


FIG. 10: (color online) This set of figures describes the DQPTs occurring following a quench across a single DP when the Semenoff mass is quenched from  $M_i = 3$  to  $M_f = 1$ . Fig. 10(a) shows that  $p_{\mathbf{k}}$  is unity only at the upper DP ( $k_x = 2\pi/3, k_y = 4\pi/3\sqrt{3}$ ) and non-zero in its vicinity while vanishing away from it; here,  $L = 100$ . As shown in Fig. 10(b), the FZs (for  $n = 0$ ) resembles a similar structure as that of the sudden quenching case [49] where the dense area intersects the imaginary (real time) axis; one observes non-analyticities in the  $\text{Re}[f'(t)]$  at the boundaries of the area as prominently shown in Fig. 10(c) choosing  $L = 1000$ . Fig. 10(d) shows the maximum and minimum value of these  $e^2(\mathbf{k}^*)$ 's correspond to  $t_b^s$  and  $t_e^s$  as obtained from Eq. (6).

the Hamiltonian

$$\begin{aligned} \mathcal{H} = & t_1 \sum_{i,j=N1} (c_{iA}^\dagger c_{jB} + h.c.) \\ & + t_2 \sum_{i,j=N2} (e^{i\phi_{ij}} (c_{iA}^\dagger c_{jA} + c_{iB}^\dagger c_{jB}) + h.c.) \quad (\text{A1}) \\ & + M \sum_{i \in A} \hat{n}_i - M \sum_{i \in B} \hat{n}_i. \end{aligned}$$

The  $c_{iA(B)}$ s are spinless fermionic operators on sublattice  $A$  ( $B$ ), and the  $t_2$ s are the next nearest neighbour hopping interaction strengths. The time reversal symmetry of this model is broken by the phase factor  $\phi_{ij} = \pm\phi$ , originating from the staggered magnetic field and is pos-

itive for anticlockwise next nearest neighbour hopping.

Fourier transforming into  $k$ -space the Hamiltonian becomes

$$\mathcal{H} = \begin{pmatrix} c_A^\dagger(\mathbf{k}) & c_B^\dagger(\mathbf{k}) \end{pmatrix} \mathbf{h}(\mathbf{k}) \begin{pmatrix} c_A(\mathbf{k}) \\ c_B(\mathbf{k}) \end{pmatrix}, \quad (\text{A2})$$

where

$$\mathbf{h}(\mathbf{k}) = \sum_{i=0}^3 h_i(\mathbf{k}) \sigma_i. \quad (\text{A3})$$

The  $\sigma_i$ ,  $i \in \{1, 2, 3\}$  are the Pauli matrices,  $\sigma_0$  is the

identity matrix and  $a$  is the lattice constant. We have

$$h_0 = 2t_2 \cos(\phi) \left[ \cos(\mathbf{k} \cdot \mathbf{a}_1) + \cos(\mathbf{k} \cdot \mathbf{a}_2) + \cos(\mathbf{k} \cdot (\mathbf{a}_1 - \mathbf{a}_2)) \right], \quad (\text{A4})$$

$$h_1 = t_1 \left[ 1 + \cos(\mathbf{k} \cdot \mathbf{a}_1) + \cos(\mathbf{k} \cdot \mathbf{a}_2) \right] \\ h_2 = t_1 \left[ \sin(\mathbf{k} \cdot \mathbf{a}_1) + \sin(\mathbf{k} \cdot \mathbf{a}_2) \right], \quad (\text{A5})$$

$$h_3 = M + M_H, \quad (\text{A6})$$

$$M_H = 2t_2 \sin(\phi) \left[ \sin(\mathbf{k} \cdot \mathbf{a}_2) - \sin(\mathbf{k} \cdot \mathbf{a}_1) + \sin(\mathbf{k} \cdot (\mathbf{a}_1 - \mathbf{a}_2)) \right], \quad (\text{A7})$$

where  $\mathbf{a}_1 = \frac{a}{2} (3, \sqrt{3})$  and  $\mathbf{a}_2 = \frac{a}{2} (3, 3)$  as shown in

Figure 9.

## Appendix B: Quenching across a single critical point

In this Appendix, we address the following question: what happens when the quenching protocol drives the system just through one gapless DP that is from the non-topological phase to the topological phase as illustrated in Fig. 1(a). The FZs resembles a similar structure as that of the sudden quenching case [49] where the dense area intersects the imaginary (real time) axis only once without any reentrant behavior (Figs. 10(a) and 10(b)). This results in two discontinuities in  $\text{Re}[f'(t)]$  at two instants of time for a single  $n(=0)$  (Fig. 10(c)), which can be derived from Eq. (6) (Fig. 10(c)). However, even in this case when  $M_H = 0$ , the areas of FZs shrink to lines.

- 
- [1] I. Bloch, J. Dalibard, and W. Zwerger, *Rev. Mod. Phys.* **80**, 885 (2008).
  - [2] M. Lewenstein, A. Sanpera, and V. Ahufinger, *Ultracold Atoms in Optical Lattices Simulating quantum many-body systems*, (Oxford University Press, Oxford (2012)).
  - [3] M. Greiner, O. Mandel, T. W. Hansch and I. Bloch *Nature* **419**, 51 (2002).
  - [4] T. Kinoshita, T. Wenger and D. S. Weiss, *Nature* **440**, 900 (2006).
  - [5] M. Gring, M. Kuhnert, T. Langen, T. Kitagawa, B. Rauer, M. Schreitl, I. Mazets, D. Adu Smith, E. Demler, and J. Schmiedmayer, *Science* **337**, 1318 (2012).
  - [6] S. Trotzky, Y.-A. Chen, A. Flesch, I. P. McCulloch, U. Schollwck, J. Eisert and I. Bloch, *Nature* **8**, 325 (2012).
  - [7] M. Cheneau, P. Barmettler, D. Poletti, M. Endres, P. Schauss, T. Fukuhara, C. Gross, I. Bloch, C. Kollath and S. Kuhr, *Nature* **481**, 484 (2012).
  - [8] D. Fausti, R. I. Tobey, N. Dean, S. Kaiser, A. Dienst, M. C. Hoffmann, S. Pyon, T. Takayama, H. Takagi, A. Cavalleri, *Science* **331**, 189 (2011).
  - [9] M. C. Rechtsman, J. M. Zeuner, Y. Plotnik, Y. Lumer, D. Podolsky, F. Dreisow, S. Nolte, M. Segev and A. Szameit, *Nature* **496** 196 (2013).
  - [10] M. Schreiber, S. S. Hodgman, P. Bordia, Henrik P. Lschen, M. H. Fischer, R. Vosk, E. Altman, U. Schneider, I. Bloch, *Science* **349**, 842 (2015).
  - [11] P. Calabrese, and J. Cardy, *Phys. Rev. Lett.* **96**, 136801 (2006); *J. Stat. Mech.* P06008 (2007).
  - [12] M. Rigol, V. Dunjko and M. Olshanii, *Nature* **452**, 854 (2008).
  - [13] T. Kitagawa, E. Berg, M. Rudner, and E. Demler, *Phys. Rev. B* **82**, 235114 (2010).
  - [14] N. H. Lindner, G. Refael and V. Galitski, *Nat. Phys.* **7**, 490-495, (2011).
  - [15] A. Bermudez, D. Patane, L. Amico, M. A. Martin-Delgado, *Phys. Rev. Lett.* **102**, 135702, (2009).
  - [16] A. A. Patel, S. Sharma, A. Dutta, *Eur. Phys. Jour. B* **86**, 1 (2013); A. Rajak and A. Dutta, *Phys. Rev. E* **89**, 042125, 2014. P. D. Sacramento, *Phys. Rev. E* **90** 032138, (2014); M. D. Caio, N. R. Cooper and M. J. Bhaseen, *Phys. Rev. Lett.* **115**, 236403 (2015).
  - [17] M. Thakurathi, A. A. Patel, D. Sen, and A. Dutta, *Phys. Rev. B* **88**, 155133 (2013).
  - [18] V. Mukherjee V. and A. Dutta, *J. Stat. Mech.* P05005 (2009).
  - [19] A. Das, *Phys. Rev. B* **82**, 172402 (2010).
  - [20] A. Russomanno, A. Silva and G. E. Santoro *Phys. Rev. Lett.* **109**, 257201 (2012); S. Sharma, A. Russomanno, G. E. Santoro and A. Dutta, *EPL* **106**, 67003 (2014).
  - [21] M. Bukov, L. D'Alessio and A. Polkovnikov, *Adv. Phys.* **64** (2016).
  - [22] A Pal and DA Huse, *Phys. Rev. B* **82**, 174411 (2010).
  - [23] R. Nandkishore, D. A. Huse, *Annual Review of Condensed Matter Physics*, **6** 15 (2015).
  - [24] J. Dziarmaga, *Advances in Physics* **59**, 1063 (2010).
  - [25] A. Polkovnikov, K. Sengupta, A. Silva, and M. Vengalattore, *Rev. Mod. Phys.* **83**, 863 (2011).
  - [26] A. Dutta, G. Aeppli, B. K. Chakrabarti, U. Divakaran, T. Rosenbaum and D. Sen, *Quantum Phase Transitions in Transverse Field Spin Models: From Statistical Physics to Quantum Information* (Cambridge University Press, Cambridge, 2015).
  - [27] J. Eisert, M. Friesdorf and C. Gogolin, *Nat. Phys.* **11**, 124 (2015).
  - [28] L. D'Alessio, Y. Kafri, A. Polkovnikov, M. Rigol, *Adv. Phys.* **65**, 239 (2016).
  - [29] M. Heyl, A. Polkovnikov, and S. Kehrein, *Phys. Rev. Lett.*, **110**, 135704 (2013).
  - [30] S. Sachdev, *Quantum Phase Transitions* (Cambridge University Press, Cambridge, UK, 2010).
  - [31] M.E. Fisher, in *Boulder Lectures in Theoretical Physics* (University of Colorado, Boulder, 1965), Vol. 7.
  - [32] C. Yang and T. Lee, *Phys. Rev.* **87**, 404 (1952).
  - [33] W. van Saarloos and D. Kurtze, *J. Phys. A* **17**, 1301 (1984).
  - [34] S. Suzuki, J-i Inoue and Bikas K. Chkarabarti, *Quantum*

*Ising Phases and Transitions in Transverse Ising Models* (Springer, Lecture Notes in Physics, Vol. 862 (2013)).

- [35] C. Karrasch and D. Schuricht, Phys. Rev. B, **87**, 195104 (2013).
- [36] N. Kriel, C. Karrasch, and S. Kehrein, Phys. Rev. B **90**, 125106 (2014).
- [37] M. Heyl, Phys. Rev. Lett., **113**, 205701 (2014).
- [38] F. Andraschko, J. Sirker, Phys. Rev. B **89**, 125120 (2014).
- [39] E. Canovi, P. Werner, and M. Eckstein, Phys. Rev. Lett. **113**, 265702 (2014).
- [40] M. Heyl, Phys. Rev. Lett., **115**, 140602 (2015).
- [41] T. Palmai, Phys. Rev. B **92**, 235433 (2015).
- [42] U. Divakaran, S. Sharma and A. Dutta, Phys. Rev. E **93**, 052133 (2016).
- [43] Z. Huang, and A. V. Balatsky, Phys. Rev. Lett. **117**, 086802 (2016).
- [44] T. Puskarov and D. Schuricht, arXiv: 1608.05584 (2016).
- [45] J. M. Zhang and H.-T. Yang, arXiv: 1605.05403 (2016).
- [46] M. Heyl, arXiv: 1608.06652 (2016).
- [47] S. Vajna and B. Dora, Phys. Rev. B **89**, 161105(R) (2014).
- [48] S. Sharma, S. Suzuki and A. Dutta, Phys. Rev. B **92**, 104306 (2015).
- [49] S. Vajna and B. Dora, Phys. Rev. B **91**, 155127 (2015).
- [50] M. Schmitt and S. Kehrein, Phys. Rev. B **92**, 075114 (2015).
- [51] J. C. Budich and M. Heyl, Phys. Rev. B **93**, 085416 (2016).
- [52] F. Pollmann, S. Mukherjee, A. G. Green, and J. E. Moore, Phys. Rev. E **81**, 020101(R) (2010).
- [53] S. Sharma, U. Divakaran, A. Polkovnikov and A. Dutta, Phys. Rev. B **93**, 144306 (2016).
- [54] T. W. B. Kibble, J. Phys. A **9**, 1387 (1976).
- [55] W. H. Zurek, Nature **317**, 505 (1985).
- [56] W. H. Zurek, U. Dorner, and P. Zoller, Phys. Rev. Lett. **95**, 105701 (2005).
- [57] A. Polkovnikov, Phys. Rev. B **72**, 161201(R) (2005).
- [58] H.T. Quan, Z. Song, X.F. Liu, P. Zanardi, and C.P. Sun, Phys.Rev.Lett. **96**, 140604 (2006).
- [59] D. Rossini, T. Calarco, V. Giovannetti, S. Montangero, R. Fazio, Phys. Rev. A **75**, 032333 (2007).
- [60] F. M. Cucchietti, *et al*, Phys. Rev. A **75**, 032337 (2007); C. Cormick and J. P. Paz, Phys. Rev. A **77**, 022317 (2008).
- [61] S. Sharma, V. Mukherjee, and A. Dutta, Eur. Phys. J. B, **85**, 143 (2012).
- [62] Lorenzo C Venuti and P. Zanardi, Phys. Rev. A **81**, 022113 (2010); Lorenzo C. Venuti, N. T. Jacobson, S. Santra, and P. Zanardi, Phys. Rev. Lett. **107**, 010403 (2011).
- [63] V. Mukherjee, S. Sharma, A. Dutta, Phys. Rev. B **86**, 020301 (R) (2012).
- [64] T. Nag, U. Divakaran and A. Dutta, Phys. Rev. B **86**, 020401 (R) (2012); S. Suzuki, T. Nag and A. Dutta, Phys. Rev. A (2016).
- [65] B. Dora, F. Pollmann, J. Fortgh, G. Zarand, Phys. Rev. Lett. **111**, 046402 (2013); R. Sachdeva, T. Nag, A. Agarwal, A. Dutta, Phys. Rev. B **90**, 045421 (2014).
- [66] A. Gambassi and A. Silva, arXiv: 1106.2671 (2011); Phys. Rev. Lett. **109**, 250602 (2012); P. Smacchia and A. Silva, Phys. Rev. E **88**, 042109, (2013).
- [67] A. Russomanno, S. Sharma, A. Dutta and G. E. Santoro, J. Stat. Mech., P08030 (2015).
- [68] P. Zanardi, H. T. Quan, X. Wang and C. P. Sun, Phys. Rev. A **75**, 032109 (2007).
- [69] R. Dorner, J. Goold, C. Cormick, M. Paternostro and V. Vedral, Phys. Rev. Lett. **109**, 160601 (2012).
- [70] S. Sharma and A. Dutta, Phys. Rev. E **92**, 022108 (2015).
- [71] N. Flaschner, D. Vogel, M. Tarnowski, B. S. Rem, D.-S. Luhmann, M. Heyl, J. Budich, L. Mathey, K. Sengstock, C. Weitenberg, arXiv:1608.05616 (2016).
- [72] M. Haldane Phys. Rev. Lett. **61**, 18, (1988).
- [73] G. Jotzu, M. Messer, R. Desbuquois, M. Lebrat, T. Uehlinger, D. Greif and T. Esslinger, Nature **515**, 237 (2014).
- [74] G. W. Semenoff, V. Semenoff, and Fei Zhou Phys. Rev. Lett. **101**, 087204
- [75] L. Privitera and G. E. Santoro, Phys. Rev. B (2016).
- [76] C. Zener, Proc. Roy. Soc. London Ser A **137**, 696 (1932); L. D. Landau and E. M. Lifshitz, *Quantum Mechanics: Non-relativistic Theory*, 2nd ed. (Pergamon Press, Oxford, 1965).
- [77] S. Suzuki and M. Okada, in *Quantum Annealing and Related Optimization Methods*, Ed. by A. Das and B. K. Chakrabarti (Springer-Verlag, Berlin, 2005), p. 185.
- [78] N. V. Vitanov and B. M. Garraway, Phys. Rev. A **53**, 4288 (1996); N. V. Vitanov, *ibid.* **59**, 988 (1999).
- [79] A. Dutta, R. R. P. Singh, and U. Divakaran, EPL **89**, 67001 (2010);
- [80] X. Peng, H. Zhou, B.-B. Wei, J. Cui, J. Du, and R.-B. Liu, Phys. Rev. Lett. **114**, 010601 (2015).